SYNTHESIS, CHARACTERIZATION AND X-RAY DIFFRACTION ANALYSIS OF ALUMINUM OXIDE NANOMATERIALS

Supported by tetfund

[1]Joseph Owolabi and [2] Pius Ojadi
[1,2]Department of Physics, Prince Abubakar Audu University, Anyigba, Kogi State, Nigeria.
Corresponding author e-mail: josedeleowo85@gmail.com

Received: September 14, 2023 **Accepted:** November 28, 2023

Abstract: This study centered on the synthesis and characterization of Al_2O_3 nanoparticles, vital for assessing material properties prior to their application in Science, Engineering, and Technology. Aluminum nanoparticles were synthesized utilizing aluminum nitrate nonahydrate and ethanol as precursors. The resulting nanoparticles underwent calcination at 1000°C for 1 h and were subsequently characterized via X-ray Diffraction (XRD). The outcomes revealed the presence of corundum (α–Al_2O_3) as a phase within the Al_2O_3 nanoparticles. The average crystallite size was determined to be 30.12 nm, accompanied by an interplanar spacing of 0.2187 nm. Dislocation analysis yielded a value of 0.000515 lines/nm², while micro-strain was calculated at 0.003701 nm^{-2}.

Keywords: Synthesis, Characterization, Aluminum oxide, XRD, Calcination.

Introduction:

Nanomaterials encompass a wide range of materials with dimensions between 1 to 100 nanometers and structures smaller than 100 nanometers. These materials exhibit unique properties based on their size and dimensionality, categorized into one-dimensional, two-dimensional, and three-dimensional structures. They are sourced from natural, anthropogenic, artificial or engineered origins. Natural nanomaterials derive from processes like photochemical reactions, volcanic eruptions, forest fires, erosion, and biological by-products (Buzea *et al*., 2007). Incidental nanomaterials stem from combustion, chemical manufacturing, welding, and other processes, while anthropogenic nanomaterials include metal oxides, zero-valence metals, quantum dots, and dendrimers (Farre and Bucelo, 2011; Buzea and Robbie, 2007).One such nanomaterial of interest is alumina (Al_2O_3) a compound composed of aluminum and oxygen. Alumina naturally appears as a white, odorless, crystalline powder, finding applications as desiccants, filters, gas sensors for environmental monitoring, coatings, paints, and environmental decontaminants (Rim, 2020; American Chemical Society, 1997). Alumina exists in various polymorphs, including gamma (γ-), delta (∂-), theta (θ-), rho (ρ-), eta (Π-), kappa (Ƙ-), and chi (χ-) alumina, with the alpha (α-) phase, known as corundum, being the most stable and useful (Digne *et al.*, 2002). Of particular interest are the alpha (α-) and gamma (γ-) phases due to their mechanical stability, chemical resistance, and high-temperature resilience. Aluminum oxide nanomaterials exhibit diverse properties that are harnessed in electronics, thermal catalysis, photonics, biosensors, and optoelectronics, evolving as their sizes approach the nanoscale (Daniel *et al*., 2004; Tian *et al*., 2004). Characterization of aluminum oxide nanoparticle properties, including phase composition, crystallite size, micro-strain, and interplanar spacing, can be achieved through techniques such as X-ray Diffraction (XRD) analysis (Owolabi, 2022).

Synthesis of Aluminum Oxide Nanoparticles:

The synthesis of aluminum oxide nanoparticles often employs the sol-gel method due to its cost-effectiveness, ability to control particle characteristics, and lower temperature requirements (Zhu et al., 2012). This chemical technique is particularly advantageous for generating metallic oxides, ceramics, and glass materials. It employs metal alkoxides or inorganic salts as precursors, undergoing hydrolysis and polycondensation reactions to form a colloidal suspension known as a sol (Chaudhury *et al.,* 2007). The sol-gel process involves transitioning a liquid "sol" into a solid "gel" phase (Mourad *et al.,* 2009). The resulting gel is subsequently dried and subjected to calcination at varying temperatures to yield the desired metal oxide nanopowder.

Materials and Methods:

Materials: All materials and reagents employed in this study were of analytical grade. A total of 10 g of aluminum nitrate nonahydrate ($Al(NO_3)2{\cdot}9H_2O$) was dissolved in 100 ml of pure water to form a solution of aluminum nitrate nonahydrate. Additionally, 3.35 g of ethanol was dissolved in 50 ml of distilled water to create an ethanol solution.

Synthesis of Aluminum Oxide Nanoparticles: The synthesis process commenced by stirring the aluminum nitrate nonahydrate solution and the ethanol solution together at room temperature for approximately ten minutes, ensuring the formation of a homogenous mixture. The mixture was then heated to 80°C for one hour to yield a viscous liquid. The temperature was further elevated to 350°C, and combustion occurred over a span of 45 minutes, leading to a significant evolution of gases and a voluminous reaction.

Calcination and Particle Formation: The resulting burned materials were subsequently ground and subjected to calcination in a muffle furnace for one hour at 1000°C, resulting in the formation of aluminum oxide (Al_2O_3) nanoparticles.

Figure 1: Sample of aluminum oxide nanoparticle.

Characterization using X-ray Diffraction (XRD): X-ray diffraction analysis was employed to characterize the synthesized aluminum oxide nanoparticles. This technique offers insights into the lattice structure of crystalline substances, providing information about unit cell dimensions, bond angles, chemical composition, and crystallographic structure of materials (IJESM, 2018). The basis of this method lies in the constructive interference of X-rays when interacting with crystalline samples.

Bragg's Law and Analysis: The X-ray beams, generated by a cathode ray tube (CRT), were filtered, collimated, and directed towards the sample. The interaction between the incident X-ray beams and the sample resulted in constructive interference according to Bragg's law, which correlates radiation wavelength, diffraction angle, and lattice spacing (Satyanarayana *et al*., 2018).

Bragg's law can be expressed as: $n\lambda = 2d\sin\theta$ --------(1)

Where:

- n: integer representing the order of diffraction,
- λ: wavelength of X-ray radiation,
- d: perpendicular distance between lattice planes,
- θ: glancing angle.

Particle Size Analysis: The Scherrer's formula was employed to calculate the particle size based on the broadening of X-ray diffraction lines (β) corresponding to specific (hkl) reflections:

$D = K\lambda / \beta\cos\theta$ ----------(2)

Where:

- D: mean size of crystalline domains,
- K: dimensionless shape factor (unity),
- λ: X-ray wavelength,
- β: line broadening at half maximum intensity,
- θ: Bragg's angle.

The size of crystalline domains (D) may be smaller or equal to the grain size.

In this study, Cu Kα radiation (λ = 1.5418 Å) was used to record the diffraction patterns, encompassing all possible diffraction directions due to the random orientation of the powdered materials.

Results and Discussion:

Morphologically, samples are crystalline and oval in shapes and the α-Al_2O_3 nanoparticle consists of hexagonal and irregular shapes of an average particle size of 17.91nm. Also the α-alumina nanoparticle is not totally agglomerated somewhat dispersed.Al_2O_3 synthesized through sol-gel method and cacined at 1000^0C showed a wavy morphology sand structure. This wavy or spiral structure might be due to some impurities and water molecules present as seen in figure 1.According to Proboriova *et al*.,(2013), the strong absorption edge between 200 – 270nm in the UV region as reported of aluminum nanoparticles. The values are in agreement with Kabayashaki *et al* (2005), and Kamil *et al*(2021).This dictates Al_2O_3 nanoparticles usefulness in diverse areas of human endeavor ranging from electronic, sensing systems, fibre optics/devices, solar cells, data memories, paint industries, chemical and biological sensors, soil and water remediation, pollution monitoring, in medicine for drug delivery systems, antimicrobial agents, Lab-on-the chip or medical rapid test, coatings and textile industries . It is worth noting that the usefulness of the nanoparticles is due to their chemical, physical and mechanical properties as a result of their fine grain sizes of 1 – 100nm. Furthermore, the shape or nanoparticles play critical role in the definition of resultant properties as well as in the strength of adhesion and cohesion. The spherical shape of a nanoparticles also enables it to have minimum surface area and assumes minimum possible state of energy in existence.

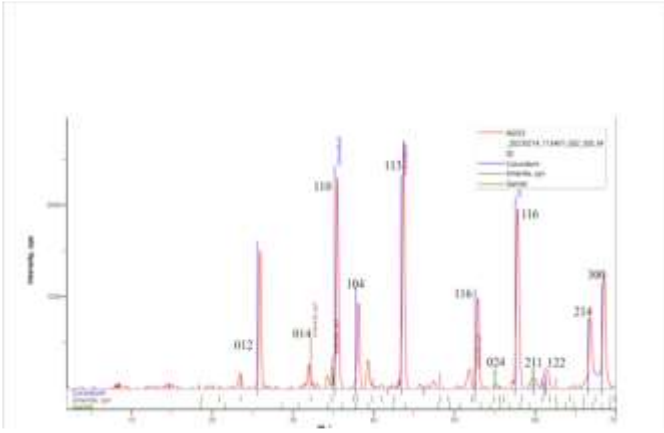

Figure 2: X-ray Diffractogram of Al_2O_3 NPS

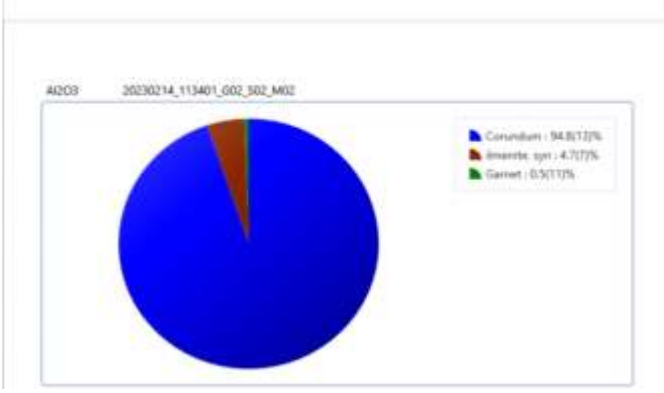

Figure 3: Quantitative analysis of Al_2O_3 NPS

Figure 3 displays X-ray Diffractogram Showing Polycrystalline Structure of Al2O3**.** This XRD plot illustrates the polycrystalline structure of Al2O3 nanoparticles, with distinct peaks corresponding to different phases and crystalline planes.

Table 1: Phases of analyzed sample of Al_2O_3 nanoparticle at 1000^0C

S/N	**Θ (degree)**	Phase Name	**FWHM (β)**	Inter - atomic Spacing(d)	**Crystalline size (nm) (D)**	**Hkl Miller Index**	Dislocation Density (δ)
1	11.69	Ilmenite	0.35	3.802	24.30	012	0.001694
2	12.98	Corundum(α)	0.258	3.430	33.00	012	0.000918
3	15.97	Ilmenite	0.15	2.8008	58.20	104	0.000295
4	17.17	Ilmenite/garnet	0.25	2.6093	35.20	110/420	0.000807
5	17.76	Corundum(α)	0.236	2.5250	36.90	104	0.000734
6	19.03	Corundum/Garnet	0.28	2.3622	31.00	110/422	0.001041
7	19.64	Ilmenite/Garnet	0.35	2.2923	25.10	113/431	0.001587
8	21.84	Corundum	0.317	2.0703	28.20	113	0.001257
9	25.91	Ilmenite	0.26	1.7628	35.90	116	0.000776
10	26.42	Corundum(α)	0.314	1.7311	29.50	024	0.001149
11	28.87	Corundum/ilmenite	0.33	1.5951	28.40	116	0.001235
12	29.85	Corundum/ilmenite	0.80	1.548	12.00	211	0.006944
13	30.63	Corundum/ilmenite	0.74	1.5119	13.00	122	0.005917
14	33.37	Corundum/ilmenite	0.35	1.4006	28.2	214	0.001257
15	34.24	Corundum	0.29	1.3690	34.30	300	0.000850

The table 1 provides information about the identified phases, their corresponding Miller indices, full width at half maximum (FWHM), inter-atomic spacing (d), crystalline size (D), dislocation density (δ), and micro-strain (ε) of the synthesized Al2O3 nanoparticles**.**

Table 2: XRD data of Al_2O_3 Nanoparticles

2θ	θ	Cos θ	Sin θ	β = FWHM (deg)	β= FWHM (rad)	βCos θ (deg.)	βCos θ (rad).	Micro Strain (ε)	d spacing (nm)	Size D(nm)
23.38	11.69	0.9793	0.2026	0.350	0.006109	0.342755	0.005983	0.007381	3.802	24.30
25.956	12.978	0.9745	0.2246	0.258	0.004501	0.251421	0.004386	0.004883	3.430	33.00
31.93	15.965	0.9614	0.2751	0.150	0.002618	0.144210	0.002517	0.001814	2.801	58.20
34.34	17.17	0.9554	0.2952	0.250	0.004364	0.238850	0.004169	0.003510	2.609	35.20
35.525	17.663	0.9529	0.3034	0.236	0.004119	0.224884	0.003925	0.003238	2.525	36.90
38.06	19.03	0.9455	0.3261	0.280	0.004888	0.264740	0.004622	0.003543	2.362	31.00
39.27	19.635	0.9419	0.3360	0.350	0.006109	0.329665	0.005754	0.004281	2.292	25.10
43.687	21.844	0.9282	0.3721	0.317	0.005533	0.294239	0.005136	0.003450	2.070	28.20
51.82	25.91	0.8995	0.4370	0.260	0.004538	0.233870	0.004082	0.002335	1.763	35.90
52.84	26.42	0.8956	0.4449	0.314	0.005481	0.281218	0.004988	0.002758	1.731	29.50
57.752	28.863	0.8758	0.4827	0.334	0.005760	0.292517	0.005045	0.002612	1.595	28.40
59.70	29.85	0.8673	0.4977	0.800	0.013964	0.693840	0.012111	0.006083	1.548	12.00
61.26	30.63	0.8605	0.5095	0.740	0.012917	0.636770	0.011151	0.005454	1.512	13.00
66.73	33.365	0.8352	0.5499	0.350	0.006109	0.292320	0.005102	0.002319	1.401	28.20
68.48	34.24	0.8267	0.5627	0.290	0.005062	0.239743	0.004185	0.001859	1.369	34.30

This table 2 presents comprehensive XRD data, including 2θ angles, corresponding θ values, cosine of θ, sine of θ, FWHM in degrees and radians, FWHM multiplied by cosine of θ in degrees and radians, micro-strain (ε), interplanar spacing (d), and crystalline size (D) calculations for each angle.

The combustion process resulted in the generation of aluminum nanoparticles along with the release of gases like CO2 and H2O, contributing to the high porosity of the resulting product. Upon calcination at 1000°C, the burned aluminum transformed into alpha (α) aluminum oxide. The identification of the synthesized product was conducted using X-ray Diffraction (XRD) analysis (Nassar et al., 2017; Nassar et *al*., 2014). The XRD analysis revealed the presence of three phases of aluminum oxides in the sample: Corundum (α-Al2O3), Ilmenite, and Garnet, each with varying percentage compositions, as illustrated in Figure 1.

The aluminum oxide nanoparticle synthesized through the sol-gel method was characterized using XRD analysis to ascertain its phase identification and purity. Heat treatment not only induced annealing in the particles but also facilitated the formation of larger grains, thereby increasing the degree of crystallinity. This heating process enabled a comparison between the diffraction patterns of the nanoparticles and bulk materials, highlighting how the shape and intensity of peaks changed across samples of different sizes (Xie and McCourt, 2008; Kamil *et al*., 2016).

The XRD spectrum of the synthesized Al2O3 calcined at 1000°C displayed distinct peaks at various 2θ angles: 23.38°, 25.96°, 31.93°, 34.34°, 35.53°, 38.06°, 39.27°, 43.69°, 51.82°, 52.84°, 57.75°, 59.70°, 61.26°, 66.73°, and 68.48°. These peaks corresponded to the Miller indices 012, 014, 110, 104, 113, 116, 024, 211, 122, 214, and 300, respectively, as indicated in Figure 3. Moreover, the XRD pattern suggested that the synthesized Al2O3 exhibited polymorphism and a pH range of approximately 1–2. Comparison with reference patterns (DB Card No: 01-077-2135, 04-012-1169, 00-002-0981) indicated the presence of multiple phases such as Corundum, Ilmenite, and Garnet (Ruby), reflecting the polycrystalline and polymorphic nature of the sample (Yul *et al*., 2006; Kamil *et al*., 2016).

Crystallite Size, Interplanar Spacing, Dislocation Density, and Micro-strain:

The crystal size was calculated using Scherrer's formula, yielding an average size of approximately 30.15 nm. Interplanar spacing, representing the distance between reflected and refracted rays, was determined to be 0.2187 nm (2.19 Å). The calculated dislocation density was 0.031231 lines/nm², and the micro-strain was evaluated to be 0.003732. These values provided insights into the structural characteristics and defects present in the synthesized aluminum oxide nanoparticles.

Conclusion:

In this study, aluminum oxide nanoparticles were successfully synthesized using the Sol-gel method and characterized through X-ray Diffraction analysis. The findings of this research shed light on the relationship between crystallinity and temperature, demonstrating that higher temperatures contribute to increased crystallinity. The synthesized nanoparticle displayed characteristics of being both polycrystalline and polymorphic, indicating various phases of alumina such as Corundum, Garnet, and Ilmenite.Through the utilization of Scherrer's equation, the particle size and crystallite diameter were calculated, revealing valuable insights into the physical properties of the synthesized aluminum oxide nanoparticles. Furthermore, the interplanar spacing, which represents the distance between lattice planes, was determined. The assessment of dislocation density within the sample was crucial in understanding defects and deformities within the crystal structure, influenced by factors such as annealing temperature and material composition.

In conclusion, this study contributes to the understanding of aluminum oxide nanoparticles' properties and characteristics. The utilization of the Sol-gel method for synthesis and X-ray Diffraction for characterization provides a valuable framework for further research and applications in various scientific and technological fields. The findings highlight the potential of these nanoparticles in diverse applications due to their unique properties and structural features.

References

1. Buzea, C., Paceheco, I.I. and Robbie, K. (2007). Nano materials and Nanoparticles: Sources and Toxicity, *Biointerphases*, 2, 17 - 172.
2. Chandhury, Z, Xu, L., Li, F. and Cheng, H. (2011). Doped graphine sheets as anode materials with super high rate and large capacity for lithium ion batteries. ACS nano 5(7), 5463-5471
3. Daniel, M.C, (2004). Gold nanoparticles: assembly, Superamolecular Chemistry, quantum-size-related properties, and applications toward biology, catalysis, and nanotechnology. Chem. Rev. 104(1): 293-346.
4. Digne, R. and Moret, M.P. (2002). Optical absorption edge of Brookite Titanium dioxide. Solid State Commun. 137(3): 154 – 157.
5. Farre and Barcelo, (2011). "Analysis and Assessment of the Occurrence, the Fate and the Behavior of Nanomaterials in the Environment", Trends in Analytical Chemistry, vol. 30, no.3, pp 517 – 527.
6. IJESM, (2018). International Journal of Engineering, Science and Mathematics 7(12).
7. Kamil, F., Hubiter, K. A., Abed, T. K. and Al–Amiery, A. A. (2016). Synthesis of Aluminum and Titanium Nanoparticles via Sol–gel Method: Optimization for the Minimum size. *Journal **of** Nanoscience Technology* 2(1), 37 – 39.
8. Kamil, F., Hubiter, K. A., Abed, T. K. and Al – Amiery, A. A.(2016). Synthesis of Aluminum and Titanium Nanoparticles via sol– gel Method: optimization for the minimum size. *Journal of Nanoscience Technology* 2(1), 37 – 39.
9. Kobayashaki, Y; Ishizaki, T. and Kurokawa, Y. (2005). Preparations of Alumina Films by Sol-gel Method. *Journal Material Science*, 4(2), 263 – 283).
10. Proboriova, Z. and Babula, P. (2013): Toxicity of Aluminum oxide Nanoparticles Using A BY- 2 Plant Cell Suspension Culture Model, Env. and Experimental control, Botany, 91: 1 – 11.
11. Mourad, C.D., Byelov, D., Petkhov, A.DV. and Matthiis de, D.A. (2009). Sol-gel Transitions and Liquid crystal Phase Transitions in Concentrated aqueous Suspensions of Colloidal gibbsite platelets. *Journal of Physical Chemistry* B 113 (34), 11604-11613.
12. Nassar, B. and Bucheli, T.D. (2017): "Occurrence, Behavior and Effects of Nanoparticles in the Environment," *Environmental Pollution*, vol. 150, no. 1, pp. 5–22.
13. Nassar, L.C., Swaminathan, C. and Sanjeeviraja, C.(2014). Synthesis of Nanocrystalline ZnO by a Microwave-assisted Combustion method. *Powder Technology* 226, 29-33.
14. Nassar, M.Y. E., Mohammed, T.Y., Ahmed, I.S and Samir, I.(2017). MGO Nanostructure via a Sol-gel Combustion Synthesis Method using Different Fuels: an Efficient Nano-adsorbent for the Removal of some Anionic Textile dyes. *Journal of Molecular Liquids* 225, 730 – 740.
15. Nassar, N.N., Rohalla, H. and Pedro P.A.(2014). Nanoparticle Technology for Heavy Oil in-situ Upgrading and Recovery Enhancement: Opportunities and Challenges. *Journal of Applied Energy*, 133. 374 – 387.
16. Owolabi, J.(2022). The Chacterization of Nanomaterials using Scanning Electron Microscopy and Environmental Applications.

Journal of Technology Innovation and Energy. ISSN: 2959 – 8809.

17. Rim, Y.S.(2020). Review of Metal Oxides Semi–conductors based thin–film Transistors for Sensor Applications. *J. Inf. Disp.*, 2L, 203 – 210.
18. Satyanarayana, M., Rajeshkhana, G. (2018). Electrocatalytic Activity of Pd20-xAgx nanoparticles embedded in carbon nanotubes for methanol oxidation in alkaline media. Journal of ACS Applied Energy Materials 1(8), 3763 – 3770.
19. Xie, Q., McCourt, F. (2008). Nanotechnology Engineering NE 320L Lab Manual, University of Waterloo, Waterloo, pp 35 – 39.
20. Yu, Y. and Tatsuma, T. (2004). Plasmon-induced photo Electrochemistry at Metal Nanoparticles supported on nanoporous TiO_2. Chem. Commun. 1810-1811.
21. Zhu et al., 2012:hu, C., Zhai, J. and Dong, S.(2012). Bifunctional Fluorescent Carbon nanodots: Green Synthesis via Soy milk and APPLICATION as metal-free Electrocatalysts for Oxygen Reduction. *Journal of Chemical* Communications 48(75), 9367- 9369.